ASSESSMENT AND CORRECTION OF TUNNEL WALL INTERFERENCE BY NAVIER-STOKES SOLUTIONS

ICAS-92-3.5.2

C. Edward Lan and C. Alan Hsing
Department of Aerospace Engineering
The University of Kansas
Lawrence, Kansas 66045

Abstract

A computational method for assessing, and correcting solid wall wind tunnel interference effects at low subsonic speeds and high angles-of-attack is presented. A mesh system representing the domain of a model in a wind tunnel is generated and used along with appropriate boundary conditions and a thin-layer Navier-Stokes solver for a flow-field simulation of the wind tunnel environment. The computed tunnel wall pressure signature is then used as boundary data for an Euler resimulation of the same wind tunnel domain without the model. This yields an "interference flow-field" which is used to derive values for $\Delta\alpha$ and Δq needed for correcting total model aerodynamic characteristics to free-air conditions. Calculated results for a wing-body-LEX model of two different sizes indicate that the primary interference effect at high lift arises from the tunnel floor in a way similar to static ground effect. The sting is found to increase the blockage correction, but to reduce the upwash effect. By comparing pressure distributions at three spanwise stations at an angle of attack of 25 deg, it is shown that wall interference is to induce more upwash inboard but to reduce the local angle of attack outboard. To show the calculated correction factors being reasonable, results for the same model of different sizes are shown to match well after correction. It is also shown that the conventional correction methods based on linear potential flow theory tend to underestimate the lift correction. However, the overall corrections for a model with a ratio of wing to tunnel cross-sectional areas being 1.59 % are small.

Nomenclature

a	local speed of sound
b_1	$= um_1 + vm_4 + wm_7 + \frac{\mu\zeta_x}{(\gamma-1)PrRe}\frac{\partial a^2}{\partial\zeta}$
b_2	$= um_4 + vm_2 + wm_5 + \frac{\mu\zeta_y}{(\gamma-1)PrRe}\frac{\partial a^2}{\partial\zeta}$
b_3	$= um_6 + vm_5 + wm_3 + \frac{\mu\zeta_z}{(\gamma-1)PrRe}\frac{\partial a^2}{\partial\zeta}$
C	tunnel cross-sectional area
CTS	closed test section
C_D	drag coefficient
C_L	lift coefficient
C_p	pressure coefficient
c_v	specific heat at constant volume
E_t	total internal energy, = $[e + (\lvert V\rvert^2)/2]$
$\hat{E},\hat{F},\hat{G}$	inviscid fluxes
e	specific internal energy, = $\int c_v dT$
J	Jacobian of spatial transformation
m_1	$= \frac{2\mu}{3Re}\left[2\left(\zeta_x\frac{\partial u}{\partial\zeta}\right)-\left(\zeta_y\frac{\partial v}{\partial\zeta}\right)-\left(\zeta_z\frac{\partial w}{\partial\zeta}\right)\right]$
m_2	$= \frac{2\mu}{3Re}\left[2\left(\zeta_y\frac{\partial v}{\partial\zeta}\right)-\left(\zeta_x\frac{\partial u}{\partial\zeta}\right)-\left(\zeta_z\frac{\partial w}{\partial\zeta}\right)\right]$
m_3	$= \frac{2\mu}{3Re}\left[2\left(\zeta_z\frac{\partial w}{\partial\zeta}\right)-\left(\zeta_x\frac{\partial u}{\partial\zeta}\right)-\left(\zeta_y\frac{\partial v}{\partial\zeta}\right)\right]$
m_4	$= \frac{\mu}{Re}\left[\left(\zeta_y\frac{\partial u}{\partial\zeta}\right)+\left(\zeta_x\frac{\partial v}{\partial\zeta}\right)\right]$
m_5	$= \frac{\mu}{Re}\left[\left(\zeta_z\frac{\partial v}{\partial\zeta}\right)+\left(\zeta_y\frac{\partial w}{\partial\zeta}\right)\right]$
m_6	$= \frac{\mu}{Re}\left[\left(\zeta_z\frac{\partial u}{\partial\zeta}\right)+\left(\zeta_x\frac{\partial w}{\partial\zeta}\right)\right]$
M	Mach number
OTS	open test section
p	static pressure
Pr	Prandtl number, = 0.72
$\hat{Q}$	conservation variables
q	dynamic pressure
Re	Reynolds number
S	wing planform area
$\hat{S}$	thin-layer viscous flux
t	time coordinate
U,V,W	contravariant velocities
U_∞,V_∞	freestream velocity
u,v,w	x, y and z velocity components
x,y,z	Cartesian coordinates directions
α	angle of attack
β	parameter controlling grid point spacing
ξ,η,ζ	curvilinear coordinate directions
μ	coefficient of dynamic viscosity
ρ	density

Superscripts:

n	denotes time level
~	denotes a dimensional quantity

Subscripts:

c	corrected
∞	denotes property at freestream conditions
x,y,z	denotes differentiation in x, y, and z directions respectively
ξ,η,ζ	denotes differentiation in ξ, η, and ζ directions respectively

I. Introduction

It is well known that due to the presence of solid wall boundaries, flow conditions which a model experiences in a wind tunnel are not the same as

those in free-air. This is particularly true for models occupying a large percentage of tunnel test section space and models at high angles-of-attack. Possible types of wind tunnel interference due to the presence of lateral solid wall boundaries are as follows[1]:

1. a reduction in the averaged downwash experienced by the model, or an increase in overall angle-of-attack;

2. a change in streamline curvature about the model, equivalent to an alteration in the camber of the model;

3. an alteration to the local angle-of-attack along the span of the model, equivalent to a change in the twist of the wing;

4. a change in dynamic pressure about the model due to "solid" and "wake" blockage;

5. buoyancy effect due to axial pressure gradient in the test section.

Other wind tunnel imperfections which must of course be accounted for are flow angularity, local variations in velocity, tare, and interference between other elements in the tunnel. These effects will not be addressed here as it is assumed that these effects have been removed before wall effects are considered. In this paper, only corrections in (1), (2) and (4) at low speeds will be considered.

In the past, linear potential flow theory has been the most widely used one in developing the correction techniques. The linear flow equation have been solved by either the method of images, or panel methods. Refs. 1 and 2 are two extensive treatises that cover how the method of images is implemented for two and three-dimensional configurations. These linear potential flow methods unfortunately cannot predict the blockage effects, and effects associated with model flow separation, such as vortex flow.

Another popular method of wall interference correction is the tunnel wall pressure signature method. This method is based on experimentally measured pressure data for an inverse simulation of the tunnel interference flow field . Using measured tunnel wall pressure data at some suitable locations, appropriate flow singularity model at the tunnel centerline can be established to produce these pressure signature. The resulting flow singularity model is then used to produce the correction factors[3]. This was called the "indirect method" in Ref. 4. If more extensive wall pressure measurements are available, a flow singularity model at the tunnel centerline is not needed. Instead, flow singularity distribution representing wall pressure disturbance can be directly used to calculate the corrections[5-8]. This was called the "direct method"[4]. In both "direct" and "indirect" methods, proper locations of wall pressure measurement are important.

To avoid measurement of wall pressure distribution, modeling of tunnel flow with the test model in the tunnel must be made. In this aspect, panel-like methods have been the most popular ones[9,10]. In Ref. 10 vortex-separated flow at high angle of attack was considered in predicting the interference corrections. However, only simple configurations, such as delta wings, were investigated and no blockage correction was predicted. High-order methods of computational fluid dynamics have also used in prediction of wall interference[7,8,11]. These investigations have been mainly concerned with the transonic flow problems, not high angle-of-attack flow.

In the present study, a theoretical method based on the thin-layer Navier-Stokes equations is used to simulate the wind tunnel interference problem. Motivation for this investigation stems from the measured discrepancy for a 76° delta wing model tested in NASA Langley's Basic Aerodynamics Research Tunnel (BART) in comparison with results from several other tunnels. BART is a small closed test section wind tunnel with a test section slightly less than 2½ feet high and 3½ feet wide. The 76° delta wing experiences much greater lift in the BART tunnel than any of the other tunnels, especially at high angles of attack. Furthermore, based on the conventional correction methods, the corrected data still failed to match other tunnel data[12]. Since the configurations of primary interest in the present investigation all involve vortex separation at high angles of attack, an appropriate choice of computational method is obviously one based on Navier-Stokes solutions. Both blockage and upwash corrections will be considered. No experimental wall pressure data will be employed. In addition to providing correction factors, another purpose of the present study is to assess the tunnel flow field to provide a basis of choosing appropriate locations of wall pressure measurement for the pressure signature method. Investigation of the 76°-delta wing was reported in Ref. 13. In this paper, a wing-body configuration in a 7-ft by 10-ft tunnel, including the effect of sting support, will be examined.

II. Theoretical Development

Governing Equations

The present flow solver is one based on ARC3D[14] and modified for the present investigation. The code solves the following thin-layer Navier-Stokes equations:

$$\frac{\partial \hat{Q}}{\partial t} + \frac{\partial \hat{E}}{\partial \xi} + \frac{\partial \hat{F}}{\partial \eta} + \frac{\partial \hat{G}}{\partial \zeta} = \frac{\partial \hat{S}}{\partial \zeta} \qquad (1)$$

where

$$\hat{Q} = \frac{1}{J}\begin{bmatrix}\rho\\ \rho u\\ \rho v\\ \rho w\\ E_t\end{bmatrix},\quad \hat{E} = \frac{1}{J}\begin{bmatrix}\rho U\\ \rho uU+\xi_x p\\ \rho vU+\xi_y p\\ \rho wU+\xi_z p\\ U(E_t+p)\end{bmatrix},$$

$$\hat{F} = \frac{1}{J}\begin{bmatrix}\rho V\\ \rho uV+\eta_x p\\ \rho vV+\eta_y p\\ \rho wV+\eta_z p\\ V(E_t+p)\end{bmatrix},\quad \hat{G} = \frac{1}{J}\begin{bmatrix}\rho W\\ \rho uW+\zeta_x p\\ \rho vW+\zeta_y p\\ \rho wV+\zeta_z p\\ W(E_t+p)\end{bmatrix} \tag{2}$$

and

$$\hat{S} = \frac{1}{J}\begin{bmatrix}0\\ \zeta_x m_1+\zeta_y m_4+\zeta_z m_6\\ \zeta_x m_4+\zeta_y m_2+\zeta_z m_5\\ \zeta_x m_6+\zeta_y m_5+\zeta_z m_3\\ \zeta_x b_1+\zeta_y b_2+\zeta_z b_3\end{bmatrix} \tag{3}$$

$$\begin{aligned} U &= \xi_x u+\xi_y v+\xi_z w,\\ V &= \eta_x u+\eta_y v+\eta_z w,\\ W &= \zeta_x u+\zeta_y v+\zeta_z w \end{aligned} \tag{4}$$

The variables, m_1, b_1, etc. are defined in Nomenclature. In the above equations, ξ represents the streamwise body-conforming coordinate, while η represents a circumferential coordinate that laterally "wraps" about the wing-body model, and ζ represents the normal coordinate to the configuration and wind tunnel wall solid surfaces. These curvilinear coordinates are related to the Cartesian coordinates through the following mapping:

$$\begin{aligned} \xi &= \xi(x,y,z)\\ \eta &= \eta(x,y,z)\\ \zeta &= \zeta(x,y,z) \end{aligned} \tag{5}$$

The basic solution methodology includes implicit time differencing and local time linearization. The finite-difference equations are then approximately factorized to give

$$\left[I+\Delta t\frac{\partial[\hat{A}]^n}{\partial\xi}\right]\left[I+\Delta t\frac{\partial[\hat{B}]^n}{\partial\eta}\right]\left[I+\Delta t\frac{\partial([\hat{C}]^n-[\hat{M}]^n)}{\partial\zeta}\right]\Delta\hat{Q}^n$$

$$= -\Delta t\left(\frac{\partial\hat{E}^n}{\partial\xi}+\frac{\partial\hat{F}^n}{\partial\eta}+\frac{\partial\hat{G}^n}{\partial\zeta}-\frac{\partial\hat{S}^n}{\partial\zeta}\right) \tag{6}$$

where the flux Jacobians are defined as

$$[\hat{A}]=\frac{\partial\hat{E}}{\partial\hat{Q}},\quad [\hat{B}]=\frac{\partial\hat{F}}{\partial\hat{Q}},\quad [\hat{C}]=\frac{\partial\hat{G}}{\partial\hat{Q}},\quad [\hat{M}]=\frac{\partial\hat{S}}{\partial\hat{Q}} \tag{7}$$

As the solution converges, $\Delta Q \rightarrow 0$ and the right hand side of Eq. (6) approaches zero. Thus, the steady Navier-Stokes equation will be satisfied. All space derivatives are expressed in central differences and Jameson's artificial dissipation[15] terms are used for numerical stability. In addition, the Balwin-Lomax turbulence model[16] is used in the method.

Boundary Conditions

In simulation of tunnel flow, boundary conditions at the upstream and downstream boundaries are similar to those of the far field in free air[8]. At solid surfaces, all velocity components are set to zero. At the interface of model and wall regions (blocks), all flow variables are extrapolated to the boundary when the velocity is outward[17]. When the velocity is inward, only the static pressure is extrapolated to smooth out the pressure distribution. Use of local one-dimensional Riemann invariants to determine boundary values was investigated and produced essentially the same results[13].

Interference Flowfield

The present method of determining the interference corrections is similar to that of pressure signature method, except that the wall pressure distribution is calculated with the Navier-Stokes solver, instead of being measured. In addition, the calculated wall pressure distribution is used as the boundary data for an Euler resimulation of tunnel domain without the model. The main objective is to generate a flow field which is compatible with the specified pressure distribution on the entire enclosing surface of the test section. This is done iteratively by extrapolating interior values of density and flow momentum and calculating total energy based on the specified pressure on the bounding surfaces. This produces an "interference flowfield" which contains $\Delta\alpha$ and Δq information that can be used to correct the measured data. The upwash correction is determined from

$$\alpha_c = \alpha+\Delta\alpha \tag{8a}$$

where

$$\Delta\alpha = \tan^{-1}\frac{\Delta w}{U_\infty+\Delta u} \tag{8b}$$

The correction to dynamic pressure is determined from

$$\frac{q_c}{q_\infty} = \frac{[(U_\infty+\Delta u)^2+\Delta w^2]}{U_\infty^2} \tag{9}$$

Grid Generation

The type of grid system that has been developed for both the wing-body configuration in free-air and in the wind tunnel is an H-O mapping. Only half of the wing-body configuration is modeled in the present investigation of symmetric flow conditions. The distribution of grid points is made such that higher concentrations of grid points are located near the leading edge of the wing. In a cross-flow plane, a quadratic curve fit is used to fit the z and y coordinates as a function of η on the wing surface grids. This quadratic fit results in a smooth grid point distribution. The sections of the trailing wake grid are arranged to have the same geometry as the last cross section of the wing and body grids. Also, the flow regions to be included in the analysis are usually extended by two body lengths fore and aft of the

model. The wing-body surface grid is rotated about the location of the model support pivot point by an angle of attack of interest, and the front and trailing wake grids are smoothly blended with the rotated wing-body grid. The surface grid for the tunnel wall is generated in a manner analogous to the wing surface grid.

The whole flow field is divided into two blocks, one around the wing-body model and the other near the tunnel wall. In both blocks, transfinite interpolation[18,19] is used to generate the interior grid points between the wing-body and outer mesh boundaries. The method is a somewhat modified form of the scheme presented in Refs. 18 and 19. This modified form produces mesh systems where grid lines propagate nearly normal to both the solid surfaces and the lateral outer mesh boundaries. To resolve better the boundary layers on the solid surfaces, in particular in turbulent flow, a coordinate stretching transformation is applied in the ζ direction. The stretching transformation is of the following form[19]

$$\zeta(\omega) = 1 - \frac{\tanh[\sigma(1-\omega)]}{\tanh\sigma} \qquad (10)$$

where ω varies uniformly from 0 to 1, and σ is given by the solution to

$$\beta = \frac{1}{\tanh\sigma} \qquad (11)$$

in which β is a parameter where the closer it is to 1, but greater than 1, the closer the grid layers will be placed near a boundary. All grids used in this investigation employ a stretching parameter of β = 1.005. In the present investigation, 50 grid lines are used in the streamwise (ξ) direction, 49 grid lines in the spanwise (η) direction and 50 grid lines in the surface-normal (ζ) direction for the block around the wing-body model. The corresponding numbers of grid lines for the outer tunnel block are 50, 49 and 16, respectively. In the present application, the flow in the outer tunnel block is always assumed to be laminar.

III. Results and Discussions

The present method was first applied to a 76-deg delta wing in the BART tunnel[13]. The results indicated that the tunnel floor surface generated most of the interference effect, similar to ground effect. The interference flow field was found to be quite nonuniform. In the present study, a wing-body configuration with a medium-sized leading edge extension (LEX)[20] will be examined. This model has been tested in a 7-ft by 10-ft tunnel. The model surface grids and the model setup in the tunnel are illustrated in Fig. 1. The sting support is also modeled in the calculation. The sting geometry is not exactly what the test set-up may indicate in Ref. 20. Instead, it is assumed to be a configuration available for the present study in a typical 7-ft by 10-ft tunnel. Since trip strips are employed on the test model, turbulent boundary layer is assumed in all calculations. Two model sizes are used in the theoretical investigation. One represents the original model as given in Ref. 20 with a ratio of wing to tunnel cross-sectional areas (S/C) being 1.59 %. The other has a S/C being 3.57 %. The calculated results to be presented in the following are organized into two parts for assessment and correction of wall interference, respectively.

Assessment of Wall Interference

(1) Wall pressure signature

Calculated wall pressure distributions are presented in Figs. 2 and 3 for both models at α = 25 deg. and M_∞ = 0.3. From Fig. 2, it is seen that the wall static pressure is relatively uniform and symmetrical around the model. The only nonuniform region is on the floor in the wake region where the sting support has large interference effect. The pressure coefficient is negative everywhere except at the entrance of the test section. This implies that the main interference effect will be blockage, not upwash change. On the other hand, the large model induces a nonuniform and nonsymmetrical (on the floor and ceiling) wall pressure distribution with a larger positive C_p below the wall and forward. Whereas C_p becomes large negative below the wake. This implies that the interference effect will be mainly upwash change, not blockage[21]. In the existing pressure signature methods, the pressure data are measured on the tunnel ceiling and floor either along the center lines[3], or several streamwise rows[5], in addition to some measuring points on the sidewalls. Fig. 3 indicates that at high lift, there should be more measuring points on the floor in the near wake.

(2) Sting effect

The presence of sting support is to modify the wake shape and the blockage effect. Its effect is illustrated in Fig. 4. The pressure distribution at α = 25 deg. is shown on the plane of symmetry. When the sting is not present, the model base flow is not modeled. The sting is replaced with a streamtube, on the upper and lower surfaces of which the flow variables are assumed to be continuous so that no loads will be generated. The results indicate that the sting changes the pressure distribution only near the aft end of the body. However, it also increases the blockage effect as will be shown later.

(3) Wall effect on wing pressure distribution

Pressure distributions calculated at α = 25 deg and M_∞ = 0.3 and y/b/2 = 0, 0.25 and 0.85 are presented in Fig. 5. It is seen that wall interference effect on the body surface is negligible (Fig. 5a), except near the body tail where the sting effect becomes important. The main wall interference effect is to

increase the LEX vortex effect at y/b/2 = 0.25 by increasing the upwash (Fig. 5b). However, near the tip there is a local reduction in α. This means that the wall interference tends to produce a washout on the wing.

Correction of Wall Interference

Based on the calculated wall pressure distribution on the lateral boundary, the interference flow field can be generated by using Euler simulation. The grid system is not changed, except that the solid-surface boundary condition is no longer specified. Typical results of this simulation at α = 25 deg. are illustrated in Figs. 6 and 7 for the two model sizes. As shown in Fig. 6a, the increase in u or dynamic pressure is not uniform. Since w/U_∞ is approximately the change in α due to wall interference, Fig. 6b indicates that there is a variation in $\Delta\alpha$ over the model. This represents the streamline curvature effect. For the large model at high lift, the blockage effect is somewhat different as shown in Fig. 7a. The increase in u is seen to be much smaller. In fact, below the model, u is slightly reduced. This is similar to static ground effect at high lift. However, the induced upwash is much higher (Fig. 7b).

To determine upwash correction, Frink[10] calculated $\Delta\alpha$ at $\bar{c}/4$ and neglected the streamline curvature effect. To correct for both effects of upwash and streamline curvature, it is suggested in the present study, based on the consideration of momentum principle, that an average $\Delta\alpha$ in the far field computed over the wake region near the center plane should be used. However, to avoid any direct sting effect, this average value will be taken in a plane at the end of the aft body when there is a sting support. Average u is always taken over the whole plane at the body tail. Finally, the following correction procedures are applied[1]:

Step 1. Divide all measured force and moment coefficients by the blockage correction factor, q_c/q_∞.

Step 2. The corrected C_L is the C_L at $\alpha + \Delta\alpha$.

Step 3. At the same corrected C_L, C_D is increased by $\Delta\alpha C_L$.

Step 4. At the same corrected C_L, add $-(\Delta C_m/\Delta\alpha)\Delta\alpha$ to the corrected C_m. This is equivalent to plotting the corrected C_m at $\alpha + \Delta\alpha$.

These correction procedures were first applied to a 76-deg delta wing in the BART tunnel and reported in Ref. 13. The corrected lift data are reproduced in Fig. 8 and are shown to agree well with the results from a 7-ft by 10-ft tunnel. In the following, results for the wing-body model will be presented.

(1) Effect of model size

It was shown in Figs 6 and 7 that model size affects significantly the interference flow field. Of interest is whether the correction factors ($\Delta\alpha$ and q_c/q_∞) obtained by the present method can correct the calculated aerodynamic characteristics to result in the same values for models of different sizes. Some calculated results are presented in Fig. 9. Except at α = 25 deg, the corrected curves of C_L, C_D and C_m for two model sizes agree very well.

(2) Effect of sting support

The results at α = 25 deg and M_∞ = 0.3 with and without the sting are compared in the following:

Sting	C_L	C_D	C_m	$\Delta\alpha$,deg	q_c/q_∞
yes	1.5196	0.7179	0.0386	0.59	1.021
no	1.4885	0.7047	0.0313	1.33	1.0

Sting	C_{Lc}	C_{Dc}	C_{mc}
yes	1.4882	0.7031	0.0378
no	1.4885	0.7047	0.0313

It is seen that the sting increases the blockage correction and reduce the upwash effect. However, the blockage-corrected C_L and C_{Di} agree well, but C_m with the sting is slightly more positive.

(3) Comparison with classical correction

Data in Ref. 20 are first "uncorrected" to obtain the "raw" data by using the method indicated in the references. On these "raw" data, the present computed corrections are then applied. The results are compared in Fig. 10. It is seen that the present corrections are slightly larger for lift. But overall, the corrections are small for this model of S/C = 1.59 %..

IV. Conclusions

A computational method has been developed for assessing and correcting tunnel wall interference effect on lift, drag and pitching moment at a low subsonic Mach number and high angles of attack. The solutions were obtained with a thin-layer Navier-Stokes solver in a body-conforming grid system. The calculated wall static pressure distribution was then used to determine the interference flowfield. Based on the latter, corrections for upwash, streamwise curvature and blockage effects were obtained. Extensive calculations were made for a wing-body-LEX configuration of different sizes in a 7-ft by 10-ft tunnel. The results indicated that at high lift, the main interference effect was from the tunnel floor, in particular in the near wake region. The sting was shown to increase the blockage correction but reduce the upwash effect. Lift increment for the present configuration in the tunnel was mainly produced in the LEX region due to increase in upwash. In the tip

region, the lift was decreased due to an induced washout. It was demonstrated that calculated results for two different model sizes could be corrected to nearly the same values by using the computed correction factors for upwash and blockage. For a small model with a ratio of wing and tunnel cross-sectional area equal to 1.59 %, the corrections were shown to be small, with the classical correction factors being lower than the present values.

V. References

1. Rae, W. H., Jr. and Pope, A., *Low Speed Wind Tunnel Testing*, John Wiley & Sons Inc., New York, 1984, pp. 344-444.

2. Garner, H. C., Rogers, E. W. E, Acum, W. E. A., and Maskell, E. C., "Subsonic Wind Tunnel Wall Corrections," AGARDograph 109, Oct. 1966.

3. Hackett, J. E., Wilsden, D. J., and Stevens, W. A., "A Review of the Wall Pressure Signature and Other Tunnel Constraint Correction Methods For High Angle-of-Attack Tests," AGARD-R-692, Feb. 1981.

4. Proctor, J. G., "Wall Pressure Signature Wind-Tunnel Wall-Constraint Correction Methods," Report BAe-ARG-188, British Aerospace, April 1984.

5. Ashill, P. R. and Keating, R. F. A., "Calculation of Tunnel Wall Interference from Wall-Pressure Measurements," *The Aeronautical Journal*, Vol. 92, Jan. 1988, pp. 36-53.

6. Mokry, M., Digney, J. R., Poole, R. J. D., "Doublet-Panel Method for Half-Model Wind-Tunnel Corrections," *Journal of Aircraft*, Vol. 24, No. 5, 1987, pp. 322-327.

7. Rizk, M. H. and Murman, E. M., "Wind Tunnel Wall Interference Corrections for Aircraft Models in the Transonic Regime," *Journal of Aircraft*, Vol. 21, Jan. 1984, pp. 54-61.

8. Rizk, M. H.; Lovell, D. R.; and Baker, T. J., "Euler Procedure for Three-Dimensional Transonic Wall Interference," *Journal of Aircraft*, Vol. 26, Jan. 1989, pp.48-55.

9. Lee, K. D., "Numerical Simulation of the Wind Tunnel Environment by a Panel Method," *AIAA Journal*, Vol. 19, April 1981, pp. 470-475.

10. Frink, N. T., "Computational Study of Wind-Tunnel Wall Effects on Flow Field Around Delta Wings," AIAA Paper 87-2420, 1987.

11. Vatsa, V. N., and Wedan, B. W., "Effect of Sidewall Boundary Layer on a Wing in a Wind Tunnel," *Journal of Aircraft*, Vol. 26, No. 2, 1989, pp. 157-161.

12. Washburn, A. E., "The Effect of Freestream Turbulence on the Vortical Flow Over a Delta Wing," Masters Thesis, George Washington University, Dec. 1990.

13. Thomas, J. P. and Lan, C. E., "The Simulation and Correction of Wind Tunnel Wall Interference on Delta Wing Lift Using Navier-Stokes and Euler Solutions," AIAA Paper 91-3300-CP, September 1991.

14. Pulliam, T. H., "Euler and Thin layer Navier Stoker Codes: ARC2D, ARC3D," *Notes for the Computational Fluid Dynamics User's Workshop*, University of Tennessee Space Institute, Tullahoma, Tennessee, Mar. 12-16, 1984.

15. Jameson, A., Schmidt, W., and Turkel, E., "Numerical Solutions of the Euler Equations by Finite Volume Methods Using Runge-Kutta Time-Stepping Schemes," AIAA Paper 81-1259, June 1981.

16. Balwin, B. S. and Lomax, H., "Thin Layer Approximation and Algebraic Model for Separated Turbulent Flows," AIAA Paper 78-257, Jan. 1978.

17. Yee, H. C., "Numerical Approximation of Boundary Conditions with Applications to Inviscid Equations of Gas Dynamics," NASA TM 81265, 1981.

18. Eriksson, L. E., "Generation of Boundary-Conforming Grids Around Wing-Body Configurations Using Transfinite Interpolation," *AIAA Journal*, Vol. 20, October 1982, pp. 1313-1320.

19. Lindeberg, T., "The Construction of a Three-Dimensional Finite Volume Grid Generator for a Wing in a Wind Tunnel with Application to Navier-Stokes Flow Solvers," FFA TN 1987-58, The Aeronautical Research Institute of Sweden, 1987.

20. Luckring, J. M., "Subsonic Longitudinal and Lateral Aerodynamic Characteristics for a Systematic Series of Strake-Wing Configurations," NASA TM 78642, February 1979.

21. Crites, R. C., "Transonic Wind Tunnel Boundary Interference - A Correction Procedure," Paper No. 15, AGARD CP 429, September, 1987.

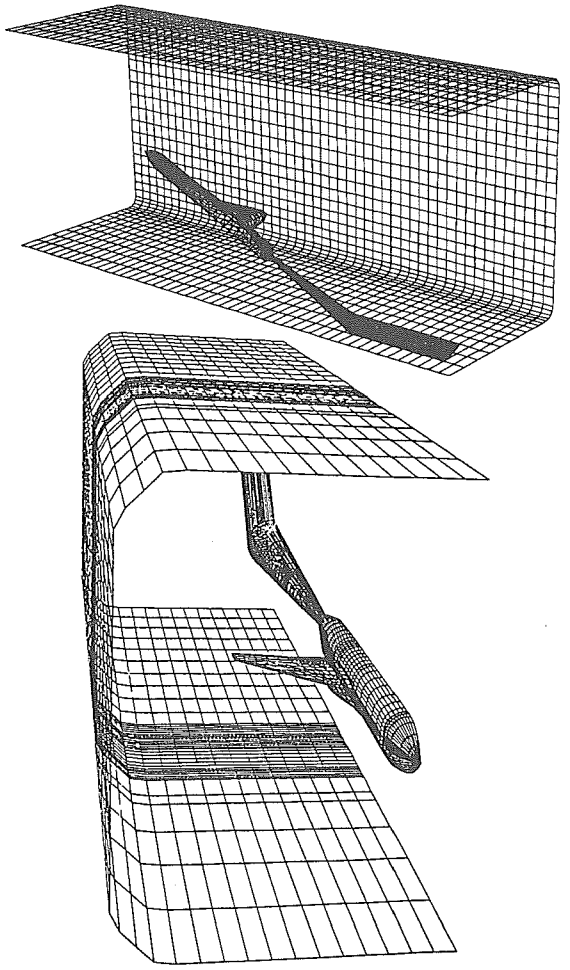

Figure 1 Computer Model of a Wing-Body-LEX Configuration in a 7-ft by 10-ft Tunnel with a Sting Support

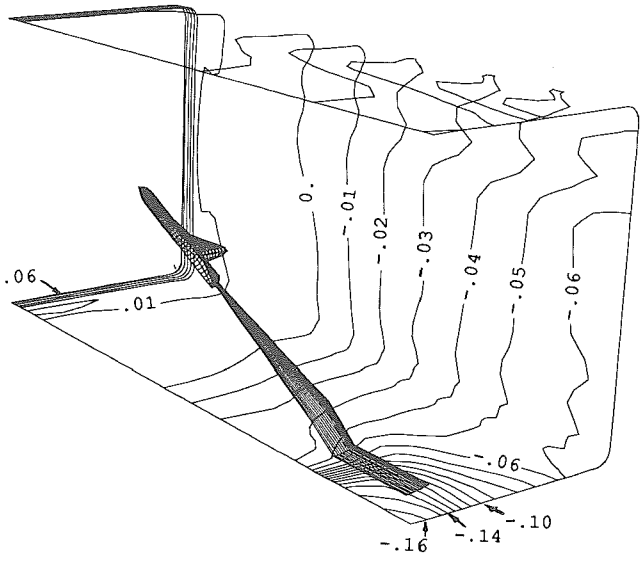

Figure 2 Computed Distribution of Wall Static Pressure Coefficients with a Small Wing-Body-LEX Configuration in a 7-ft by 10-ft Tunnel at α = 25 deg. and M_∞ = 0.3. Re = 1.3×10^6

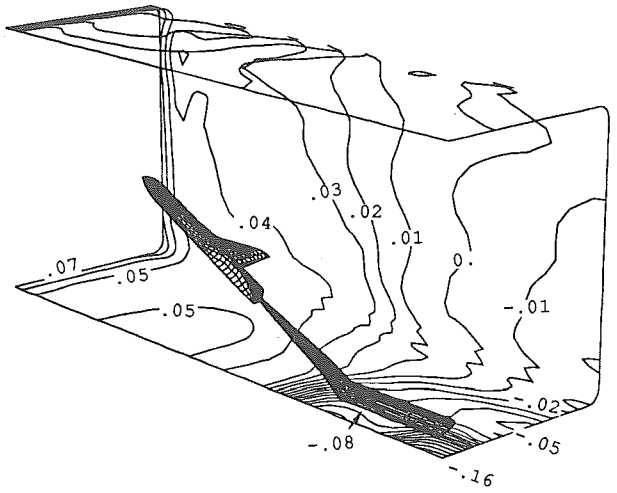

Figure 3 Computed Distribution of Wall Static Pressure Coefficients with a Small Wing-Body-LEX Configuration in a 7-ft by 10-ft Tunnel at α = 25 deg. and M_∞ = 0.3. Re = 1.95×10^6

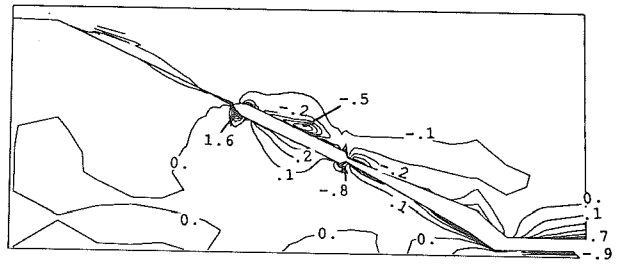

With Sting

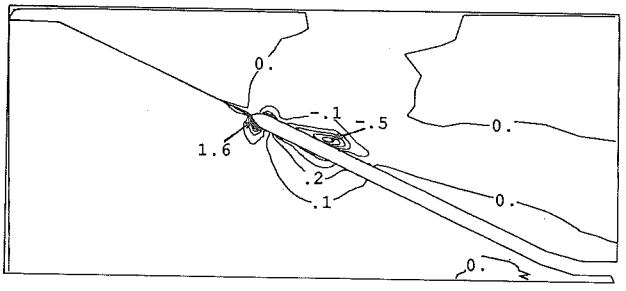

Without Sting

Figure 4 Effect of Sting Support on Pressure Distribution (C_p) on the Body on the Plane of Symmetry at α = 25 deg and M_∞ = 0.3. Re = 1.3×10^6

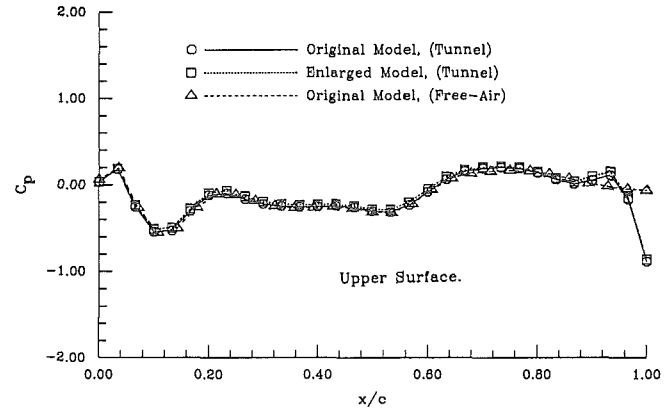

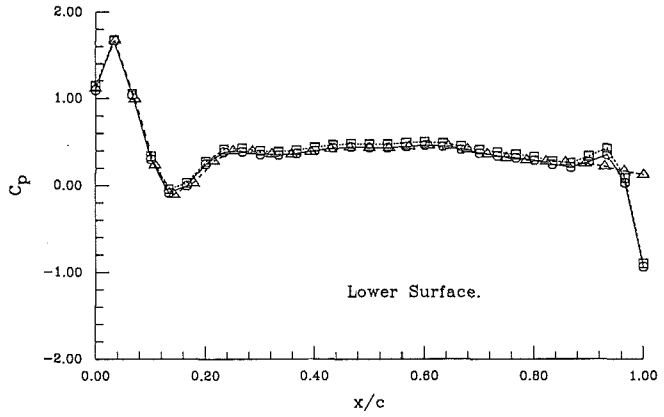

(a) y/b/2 = 0.

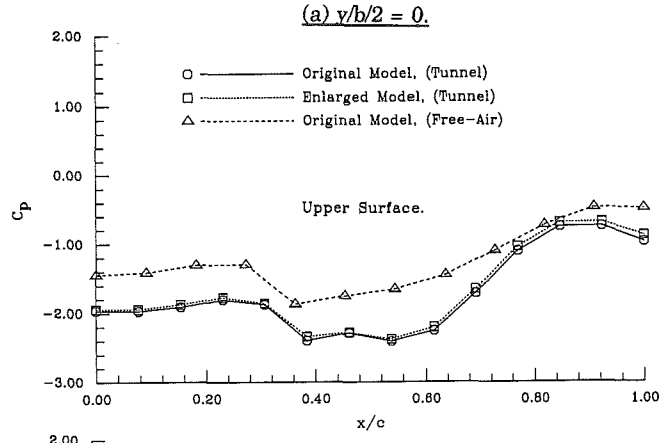

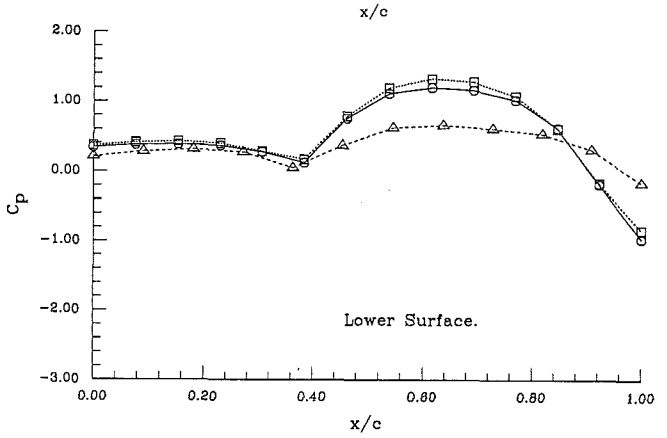

(b) y/b/2 = 0.25

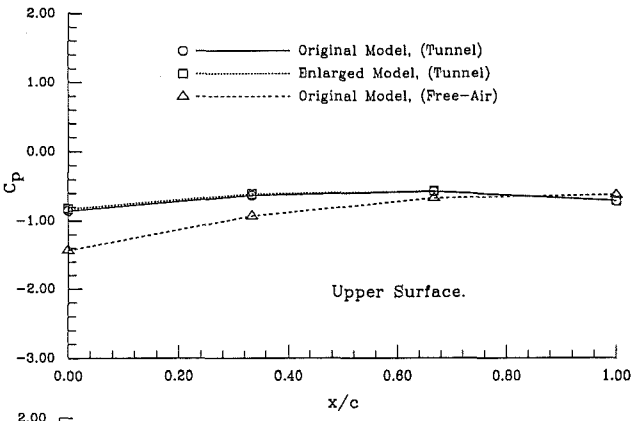

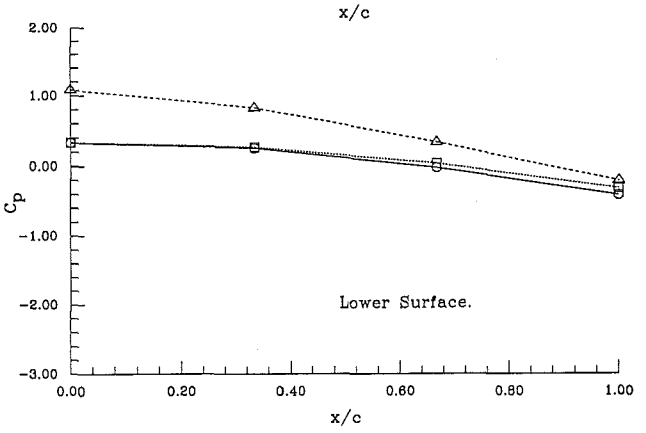

(c) y/b/2 = 0.85

Figure 5 Effect of Wall Interference on Pressure Distribution at α = 25 deg and M_∞ = 0.3

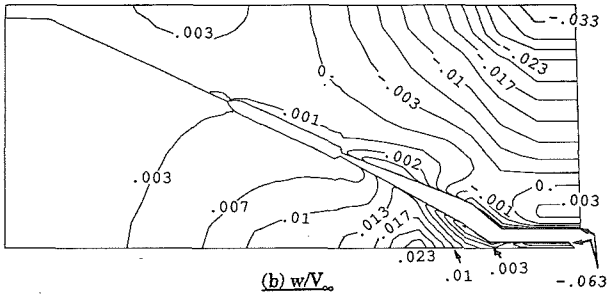

(b) w/V_∞

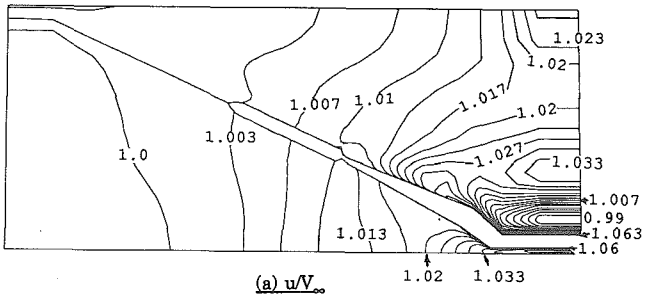

(a) u/V_∞

Figure 6 Interference Flowfield for the Small Model with S/C = 1.59 % at α = 25 deg and M_∞ = 0.3. Re = 1.3×10^6

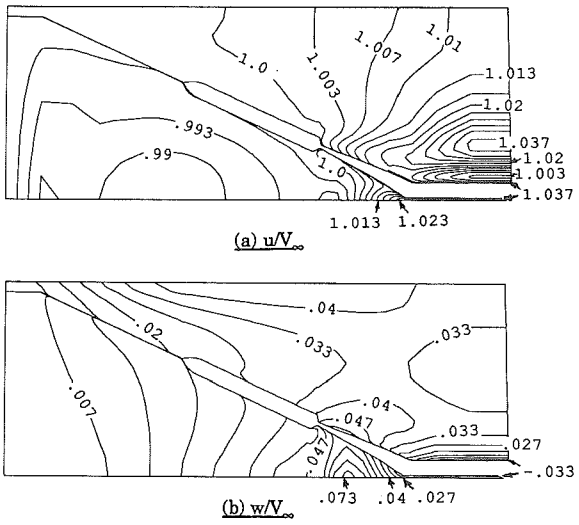

Figure 7 Interference Flowfield for the Large Model with S/C = 3.57 % at α = 25 deg and M_∞ = 0.3. Re = 1.95×10^6

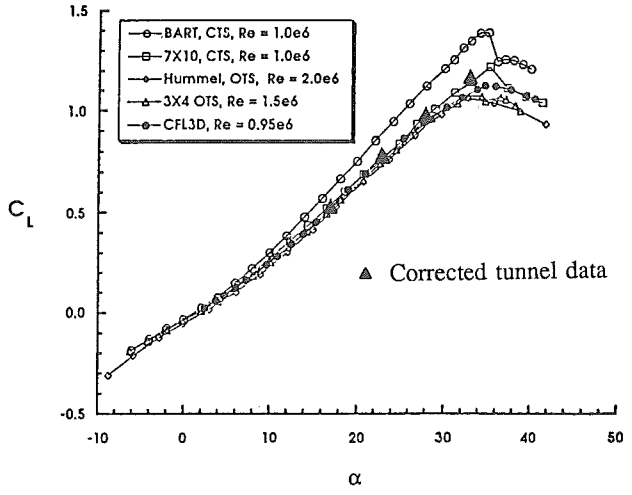

Figure 8 Comparison of Corrected Lift Curve with Other Lift Data for a 76-deg Delta Wing at M_∞ = 0.2

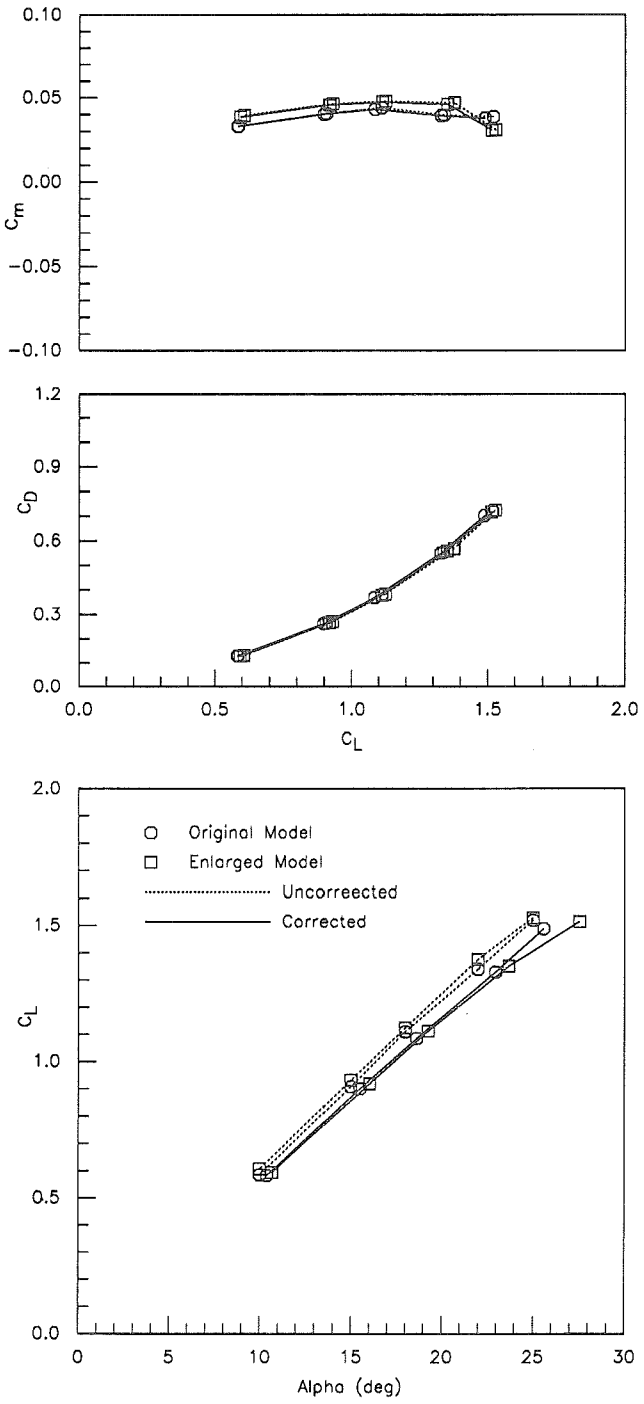

Figure 9 Wall Interference Corrections for Two Different Model Sizes at M_∞ and Re = 1.3×10^6 (Small Model) and 1.95×10^6 (Large Model)

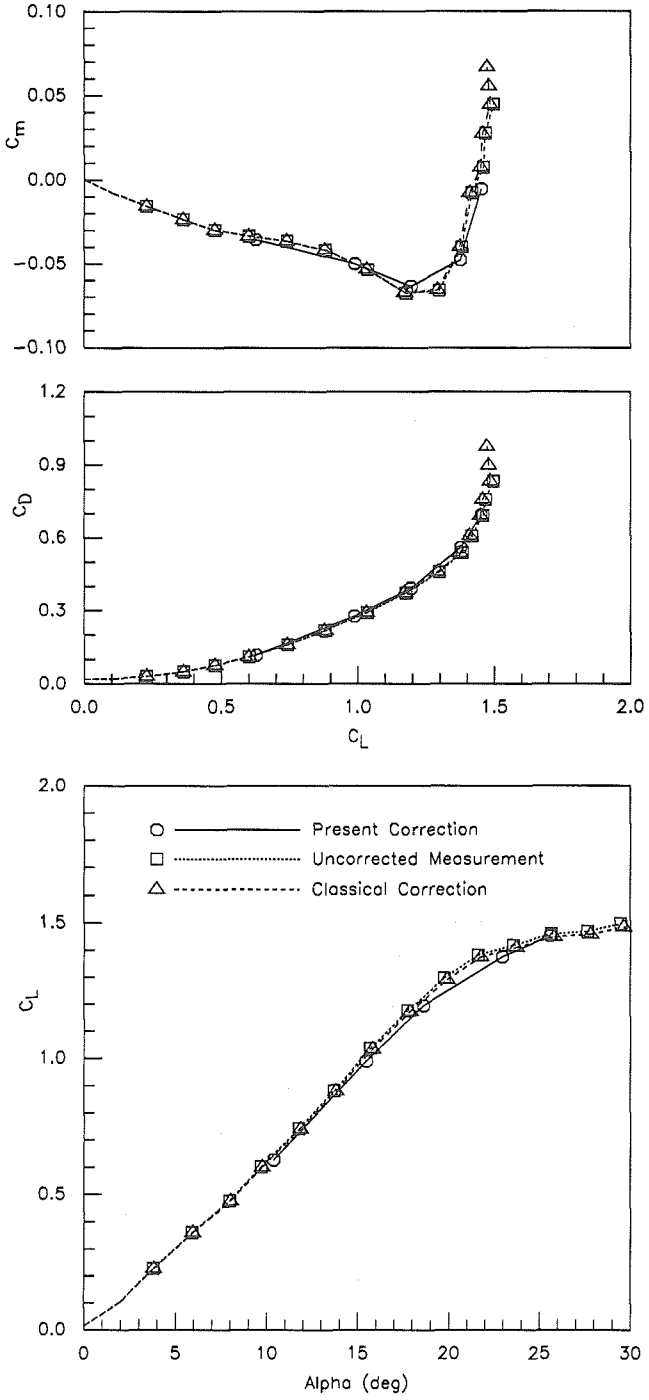

Figure 10 Comparison of Corrected Longitudinal Characteristics for the Small Model at $M_\infty = 0.3$ and $Re = 1.3 \times 10^6$.